Surfaces and Interfaces 54 (2024) 105228

Contents lists available at ScienceDirect

Surfaces and Interfaces

journal homepage: www.sciencedirect.com/journal/surfaces-and-interfaces

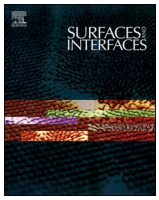

Physical and chemical surface modification by laser polishing of CuZn42 parts produced by laser powder bed fusion

Andrea Gatto [a], Riccardo Groppo [b], Maria Laura Gatto [c,*], Eleonora Santecchia [c], Daniel Munteanu [d], Paolo Mengucci [e,f]

[a] Department of Engineering "Enzo Ferrari", Università Di Modena E Reggio Emilia, Modena 41121, Italy
[b] 3D4MEC S.R.L, Via Porrettana 48, Sasso Marconi, BO 40037, Italy
[c] Department DIISM, Università Politecnica delle Marche, Via Brecce Bianche 12, Ancona 60131, Italy
[d] Material Science Department, Transilvania University of Brasov, 29 Eroilor Blvd, Brasov 500036, Romania
[e] Department SIMAU and UdR INSTM, Università Politecnica Delle Marche, Via Brecce Bianche 12, Ancona 60131, Italy
[f] UDR INSTM, Via G. Giusti 9, Firenze 50121, Italy

ARTICLE INFO

Keywords:
Laser beam powder bed fusion
CuZn42 alloy
Lead-free brass
Laser polishing
X-ray diffraction
Electron microscopy

ABSTRACT

The widespread use of Cu-Zn alloys containing lead (Pb) in plumbing applications poses significant health risks due to potential Pb leaching into drinking water. In response to international legislation aimed at reducing or eliminating Pb in metal alloys, there is an increasing demand for environmentally friendly brass. In this experimental work, authors show that during the Laser Beam Powder Bed Fusion (PBF-LB) process of the CuZn42 (CW510L) alloy, small particles only a few microns large mixed with large particles that are hundreds of microns in size, are spattered from the material. Large particles show average Zn/Cu ratio around 0.22, while for small particles it increases up to 3, against a nominal value of 0.72 for the CW510L alloy. The fallout of such particles on the produced part enriches surface of Zn, thus altering the surface chemical composition with an increase in Zn concentration beyond the acceptance limit of 43 at.%. To restore the standard chemical composition of the surface, a treatment based on the ablation of the surface material by a laser beam was proposed. Results clearly show that, after the laser treatment, the chemical composition of the surface is completely restored, and the standard properties recovered.

1. Introduction

Cu-Zn alloys are widely used in industry for their deformability, machinability, high corrosion resistance, low friction coefficient, and diamagnetism. Lead (Pb) is commonly added to these alloys to enhance machinability, increase tool life, and facilitate chip fracturing, thereby reducing manufacturing costs and minimizing machining interruptions [1]. However, leaded Cu-Zn alloys pose significant health risks in plumbing applications due to potential Pb dissolution in drinking water [2,3]. As a consequence, the interest in new Pb-free Cu-Zn alloys stimulates the research of eco-friendly materials, such as CW510L [4–8].

The higher machining costs, increased energy consumption, and lower chip control of eco-friendly brass [4], along with the requirement for preliminary release tests, drive the adoption of Additive Manufacturing (AM) technologies for producing prototypes and pre-series of valves, taps, and hydraulic devices. AM, particularly suited for small-lot and prototype production, combined with new Pb-free Cu-Zn alloys, can boost the development of new products. Among AM technologies, Laser Beam Powder Bed Fusion (PBF-LB) is capable of processing brasses with low Pb and high Zn content [9].

Although, a number of papers are present in literature dealing with Cu-Zn alloys there is still a lack of knowledge on the chemical modifications induced by Zn vaporization when Cu-Zn alloys are processed by high laser surface energy density, as occurring in PBF-LB. Furthermore, literature data report numerous papers dealing with AM of bronze, but few papers are available investigating brass [5], and most of them focus on low Zn-containing brass (red Brasses). Copper alloys with different alloying elements or Zn percentages exhibit different behavior during AM processes. The high Zn content in Cu-Zn alloys enhances Zn vaporization effects, thus originating compositional variations during the layer-by-layer growth of the component processed by AM technologies. Hugger et al. [10] evidenced zinc evaporation effects on the

* Corresponding author.
E-mail address: m.l.gatto@univpm.it (M.L. Gatto).

https://doi.org/10.1016/j.surfin.2024.105228
Received 29 May 2024; Received in revised form 24 September 2024; Accepted 4 October 2024
Available online 5 October 2024

key-hole shape during laser welding of the CuZn37 brass. The melt pool selective vaporization during laser processing causes loss of most volatile alloying elements (selective dealloying). Yin et al. [5] observed that loss of high vapor pressure elements is common to several alloys processed by laser high energy density: Mg and Zn for aluminum alloys, Cr and Mn for high-manganese stainless steels, and Zn for brass. They also studied CuZn10 components produced by PBF-LB and evidenced the vaporization effects on the chemical and physical features of the manufactured parts. Kovivchak et al. [11] observed Zn depletion of the LS59–1 brass (42% Zn) on a surface treated by ion beam. Alloying element vaporization occurs when the evaporation pressure overcomes surface tension as well as hydrostatic and hydrodynamic effects. A second mechanism causing dealloying is micro explosions occurring in the melt pool. Local micro explosions happen due to the liquid fluctuation that causes a sudden variation of transmission heat exchange surface, causing rapid local heating. The power gradient of the laser spot (TEM00) promotes Marangoni flow and spattering-inducing hydrodynamic behavior (liquid fluctuation) of the melt pool [12,13].

Yin et al. [5] evidenced that for Cu–10 Zn alloy in the range 1700 K–2930 K, the Zn saturated vapor pressure is 1–4 orders higher than Cu. These values have a substantial effect on spattered and condensed material production, causing loss of volatile elements and selective vaporization. Liu et al. [14] studied the composition of the laser ablated material from a CuZn35 alloy. They showed that particles produced by the laser action can be catalogued as ejected molten droplets and droplets condensed from vapor. Furthermore, they found a dependence of the Zn/Cu ratio on the size of the ablated particles. Smaller particles, originating from vapor condensation, are enriched with high vapor pressure elements, while larger particles are ejected from the melt pool. The larger particles have a different composition from the bulk because the melt pool is depleted of the volatile elements. Vaporized droplets from the most volatile elements may condense on the surface of the larger particles ejected from the melt.

During the PBF-LB process, droplets of variable size may fall on unmelted areas or on areas that are going to be melted by the laser, thus interacting with the melt pool after landing [15], or they may be captured by the inert gas flow and carried away from the build area.

The fallout of droplets locally modifies the surface chemical composition of the manufacturing part, whose outer surface result to be enriched of Zn with respect to the core. Building in a spatter-rich environment may be a severe problem for the effectiveness of the process [16]. Therefore, to restore the chemical composition of the part, it is necessary to remove its outer skin.

Conventional finishing processes such as peening, hand polishing and electrochemical polishing are expensive and time-consuming. Moreover, they are economically ineffective for pre-series and components with complex geometry [17,18]. A different approach could be laser polishing, which is generally used to improve the surface quality of the manufactured part by reducing roughness. Laser polishing uses thermal energy to smooth rough surfaces by melting a thin material layer. Some authors have suggested that in laser polishing treatment of the surface, the molten material removed from the peaks of the rough surface is distributed in the valleys without any loss of material. [19]. This mechanism is generally accepted, but it does not explain what happens when an alloy with a low-boiling-point component is treated. The vast literature on Laser Polishing application of metallic 3D printed components predominantly deals with Steels, Al alloys, Co-Cr alloys, Ni-base superalloys, and Ti alloys. For such materials, literature data reports a reduction of average roughness up to 80 % [20–22]. However, the literature data cannot be used to explain what happens in applications based on the CW510L alloy [17]. In this case, during the laser action, the high vapor pressure of Zn causes its vaporization, that leads to Zn depletion of the melt pool and Zn enrichment of the surface of the manufactured part. Changes in the chemical composition affects physical and chemical properties of the material [23–26]. Therefore, in the case of alloys containing highly volatile elements, post-treatment must not only improve roughness but also be able to change the chemical composition of the surface.

In a previous experimental paper [9], we have demonstrated that the CuZn42 (CW510L) alloy can be processed by PBF-LB by careful control of the printing parameters. In this experimental work, we show that during the PBF-LB process of the CW510L alloy, small and large particles, with different chemical composition, are spattered from the material. The fallout of such particles on the produced part enriches surface of Zn, thus changing the surface chemical composition. To restore the standard chemical composition of the surface we propose a treatment based on the ablation of the surface material by a laser beam. Results clearly show that, after the laser treatment, the chemical composition of the surface is completely restored, and the standard properties recovered.

2. Experimental method

2.1. Specimen manufacturing

A gas atomized CW510L powder provided by AMP GmbH Advanced Metal Powders was processed by a 3D4BRASS (3D4MECH S.r.L., Sasso Marconi, Bologna, Italy) Laser Beam Powder Bed Fusion (PBF-LB) manufacturing system to produce cubes of size $12\times12\times12$ mm^3. The raw powder was virgin and has been processed after furnace drying at 80 °C for 24 h. The chemical composition of the raw powder is compatible with the composition limits for drinking water components, reported in Table 1.

The 3D4BRASS processing system was equipped with a 300 W Yb fiber laser operating in a continuous flow of nitrogen gas. The nitrogen gas, used as protective atmosphere inside the manufacturing chamber, was produced by a local on-board generator. Preliminary tests evidenced that spattered particles captured by the protective flowing gas can preclude the efficiency of the filters of the manufacturing system. Therefore, a cyclone was placed before the battery of filters. The inclusion of this low-pressure droplet abatement system protected the battery filters from inefficiency, thus allowing black powder to be easily captured. This solution allowed collecting small (< 10 μm) and large (> 100 μm) size particles separately. The production process would stop if the oxygen content inside the chamber exceeded 0.2 percent.

Based on the results obtained in our previous study [9], the process parameters reported in Table 2 were adopted to manufacture three full-dense cubes for each combination of the six process parameters. Layer thickness of 50 μm allows for a good compromise between production time and quality of the as-manufactured bulk sample.

The building process occurred on the top of a support structure from a steel baseplate, using a standard raster scanning strategy with an 80-deg rotation between layers. Along with the raster scanning, pre-contour and post-contour passes on the outer edge of each pass were completed.

In this study, results are discussed in terms of surface energy density (SED) instead of volume energy density (VED), because preliminary tests performed on the CuZn42 alloy by using a single laser path in our manufacturing system showed that the melted zone depth ranged from five to six-layer thickness t. Thus, single-layer thickness t does not represent a significant value for data comparison, as the actual melted layer thickness varies with laser power and scanning speed. Consequently, VED does not effectively correspond to energy absorbed by the

Table 1
CW510L composition limits for drinking water component, Procedure for the acceptance of metallic materials for PDW, 12th Revision, 14th October 2019 [3].

Constituents		Impurities					
Cu [%]	Zn [%]	Al [%]	Fe [%]	Ni [%]	Pb [%]	Sn [%]	other
57.0–59.0	Bal.	≤ 0.05	≤ 0.3	≤ 0.2	–	≤ 0.3	≤ 0.02

Table 2
Process parameters used to produce specimens; Power (P), scanning speed (v), hatching space (h), layer thickness (t) and surface energy density (E_s).

Sample name	P [W]	v [mm/s]	h [mm]	t [mm]	E_s [J/mm^2]
P190V200	190	200	0.1	0.05	9.5
P190V600	190	600	0.1	0.05	3.2
P190V800	190	800	0.1	0.05	2.4
P270V200	270	200	0.1	0.05	13.5
P270V600	270	600	0.1	0.05	4.5
P270V800	270	800	0.1	0.05	3.4

unit volume of powder layer.

2.2. Surface laser polishing treatment

Three out of four lateral faces of each specimen were treated by a pulsed fiber laser (Wuxi Raycus Fiber Laser Technology CO., LTD.) with beam quality M^2 <1.8, average power P = 47 W and wavelength λ = 1060–1085 nm (Table 3). Fig. 1 shows the schematics of the cube specimen inside the production chamber, supported on the bottom plate of the manufacturing system.

Lateral faces of the cube are numbered from 1 to 4, while the face T is the top surface of the specimen, that is the last layer of material processed in the build direction. Face 1 faces the opening of the production chamber of the manufacturing system and was not submitted to the laser polishing treatment. Top and bottom surfaces of the cube differ from the lateral surfaces for absence of the staircase effect and presence of the removed supports marks, respectively. For such reasons top and bottom surfaces have been excluded from this investigation. From preliminary characterizations of lateral faces carried out before the polishing treatment, no significative differences in terms of surface topography and chemical composition were found. Thus face 1 was considered as reference.

The laser polishing process consisted in a first treatment common to faces 2, 3 and 4 of the cube (Fig. 1) with a laser frequency ν = 55 kHz (Step 1). Then a second treatment at ν = 75 kHz and ν = 100 kHz (Step 2) was carried out on faces number 3 and 4, respectively. Details of the surface polishing treatment on the lateral faces of the cube are reported in Table 3.

2.3. Structural and chemical characterization

A Scanning electron microscope (SEM) Tescan Vega 3 equipped with an EDAX Elements energy dispersive microanalysis (EDS) system was used to investigate the surface morphology and the chemical composition of the cube faces submitted to the laser polishing treatment.

A Bruker D8 Advance diffractometer operating at V = 40 kV and I = 40 mA, with Cu-Kα radiation, in the angular range 2θ = 20°– 80° was used for X-ray diffraction (XRD) analysis. Peak indexing of the XRD patterns was carried out by the DIFFRAC.EVA (Bruker) software package by using the ICDD—PDF 2 database. Shape analysis of XRD peaks was carried out by the OriginPro 2024 software package, while estimation of the phase concentration in the samples was performed by Rietveld analysis using the MAUD (Material Analysis Using Diffraction,

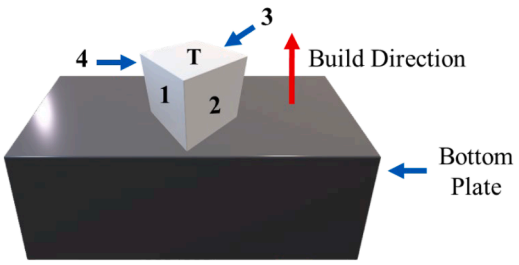

Fig. 1. Schematics of the cube lateral faces treated by the laser polishing system. The bottom plate, the top surface of the specimen and the build direction are also reported.

http:/maud.radiophema.com/) software, after calibration of the instrumental broadening by reference Al_2O_3 powder. For the Rietveld refinement the following phases were considered: 1) α-brass $Cu_{0.64}Zn_{0.36}$, cubic, space group Fm-3 m (225), nominal lattice parameter a = 0.369612 nm (ICDD-PDF2 file n. 50–1333), 2) β-brass CuZn, cubic, space group Pm-3 m (221), nominal lattice parameter a = 0.294800 nm (ICDD-PDF2 file n. 02–1231), 3) γ-brass Cu_5Zn_8, cubic, space group I-43 m (217), nominal lattice parameter a = 0.886000 nm (ICDD-PDF2 file n. 25–1228), 4) Zn, hexagonal, space group P63/mmc (194), nominal lattice parameters a = 0.266500 nm and c = 0.494700 nm (ICDD-PDF2 file n. 04–0831), 5) ZnO, hexagonal, space group P63mc (186), lattice parameters a = 0.324982 nm and c = 0.520661 nm (ICDD-PDF2 sile n. 36–1451). All XRD pattern are reported in square root intensity scale to enhance low intensity peaks.

2.4. Roughness

The surface roughness of the as-built specimen surfaces and the polished ones was measured according to DIN EN ISO 4287/4288 and DIN EN ISO 25,178 and by a Nikon LV 150 Confovis Microscope instrument using the following parameters: 20X microscopic objective; 0.595 μm lateral resolution; Scanned area of 0.5 × 1.5 mm^2; Map form removal, GAUSS filter (ISO 16,610–62) with a cut off of 2.5 μm for 2.5 μm, and bilateral symmetric threshold filtering (for removing the spikes).

The maps (ISO 25,178) allowed estimating the following parameters: a) Average surface roughness Sa; b) Surface skewness Ssk. and c) Surface kurtosis Sku.

Surface skewness assesses the incidence of valleys and peaks. For values of Ssk > 0 peaks prevail, otherwise depressions prevail. For Ssk = 0, peaks and valleys are symmetrically distributed around the mean plane. Surface kurtosis evaluates the sharpness of profiles. A normal distribution has a kurtosis value Sku = 3, while Sku<3 and Sku>3 indicate a distribution biased above the mean plane and a spiked distribution, respectively.

Table 3
Treatment type and parameters used in the laser polishing process. P - average power, t_p – single pulse duration, λ – wavelength, E_p – single pulse energy at 50 Hz. Number of the treated face refers to the schematics in Fig. 1.

Treatment name	Treated Face (ref. Figure 1)	Frequency (kHz)		P (W)	t_p (ms)	λ (nm)	E_p (mJ)
		Step 1	Step 2				
AM = As Manufactured	1	–	–	–	–	–	–
SS = Single step treatment	2	55	–	47	218	1060 - 1085	1
DS75 = SS + laser treatment at 75 kHz	3	55	75				
DS100 = SS + laser treatment at 100 kHz	4	55	100				

3. Results and discussion

3.1. Virgin raw and black powders

Morphology of the particles in the raw powder can be observed in Fig. 2A, while Fig. 2B shows the XRD pattern with the weight amount of each phase, as provided by the Rietveld refinement. The size distribution of powder particles evaluated by a laser-based granulometry system according to ISO 13,320 provided an average diameter size $d = 41$ μm. As shown in Fig. 2B, the virgin raw powder is mainly formed of β-brass (78 wt.%) with lower amounts of γ-brass (18 wt.%) and α-brass (4 wt.%).

The role of the cyclone pre-filter inserted before the filtering system of the manufacturing machine was collecting large particles, while small particles were collected in the filter. Therefore, on exclusion of the cyclone pre-filter from the filtering system all particles captured by the nitrogen gas flow were collected by the filter, independently on size. In this case, the result of the filtering action was a powder, here named "black powder", formed of particles with a wide size range, from few microns to few hundred microns. The aspect of the black powder collected in the filter on exclusion of the cyclone pre-filter is shown in the SEM image of Fig. 3A, while Fig. 3B reports the XRD pattern of the black powder with the estimated amounts of phases with the experimental errors (in wt.%), as provided by Rietveld refinement.

As shown in Fig. 3A, particles that are hundreds of microns in size are mixed with particles that are only a few microns large. EDS analysis performed in spot mode on large and small particles of the black powder showed that the Zn/Cu ratio depends on the particle size. Large particles show average Zn/Cu ratio around 0.22, while for small particles it increases up to 3, against a nominal value of 0.72 for the CW510L alloy. These results support the model of Yin et al. [5] based on the dual origin of the spattering: vaporization and explosion, as well as the findings of Liu et al. [14] on the correlation between size and composition of the spattered particles. The irregular shape of the large particles suggests that they are originated from the explosion mechanism of the melt pool rather than from vaporization. The laser action caused evaporation of Zn, which is the element of the CW510L alloy with the lowest value of vapor pressure. Then, the localized overheating due to the hydrodynamic behavior of the melt pool caused Zn vapor rapid expansion (explosion) and ejection of droplets (large particles) depleted in Zn. On the surface of the large Zn-depleted particles condensed nanometer particles almost entirely composed of Zn, originated from the vaporization action of the laser beam.

The XRD pattern in Fig. 3B shows that the black powder is formed of Zn and ZnO without any evidence of crystallized Cu-containing compounds, although the presence of such compounds cannot be completely excluded. The high amount of ZnO (95 wt.%) in the black powder is probably due to the oxidation of the powder during the operation of opening the filter box to remove the black powder.

3.2. As manufactured and treated surfaces

Structural characterization by XRD, SEM and EDS analysis was carried out on the treated and untreated faces of all samples analyzed. The results of XRD analysis showed that all samples after the polishing treatment contained only α-brass and β-brass phases, independently on the sample composition before treatment, as shown in Fig. 4. The laser action causes powder melting and Zn vaporization, which reduces the Zn content and consequently the Zn/Cu ratio in the melt pool. The reduced Zn content suppresses the formation of the γ phase in favour of the α and β phases during cooling. In our previous work [9], we found a correlation between the relative amount of α and β phases and the energy delivered to the sample during the laser action, confirming this mechanism.

In all samples analyzed, the resulting amount of α and β phases after polishing depends on the type of polishing treatment (SS, DS75, DS100). As a general trend, all samples showed an increase in the weight fraction of α-brass according to the type of polishing treatment in the sequence SS, DS75, DS100. This general trend is independent on the amount of α phase in the untreated sample (AM), thus suggesting that variation in the phases content must be ascribed to the laser polishing treatment. In our previous work [9] dealing with the PBF-LB manufacturing of parts based on the CuZn42 alloy, we reported on the variation of α and β phases fraction as a function of surface energy density (SED) and laser power (P), showing that the mechanisms involved depends on both manufacturing parameters. Therefore, the general trend evidenced in this work for the treated samples can be summarized as in Table 4, where results of the Rietveld refinement carried out on the XRD patterns of Fig. 4 are shown for the laser polished samples produced with the lowest (E_s=2.4 J/mm^2) and the highest (E_s=13.5 J/mm^2) values of SED at $P = 190$ W and $P = 270$ W.

The increase of the α phase amount with the increase of the laser frequency of the polishing treatment is due to the weight loss of Zn induced by the laser action. It is worth noting that the Zn/Cu ratio for the α phase is 0.61, while for the β phase Zn/Cu = 1.07. Therefore, a

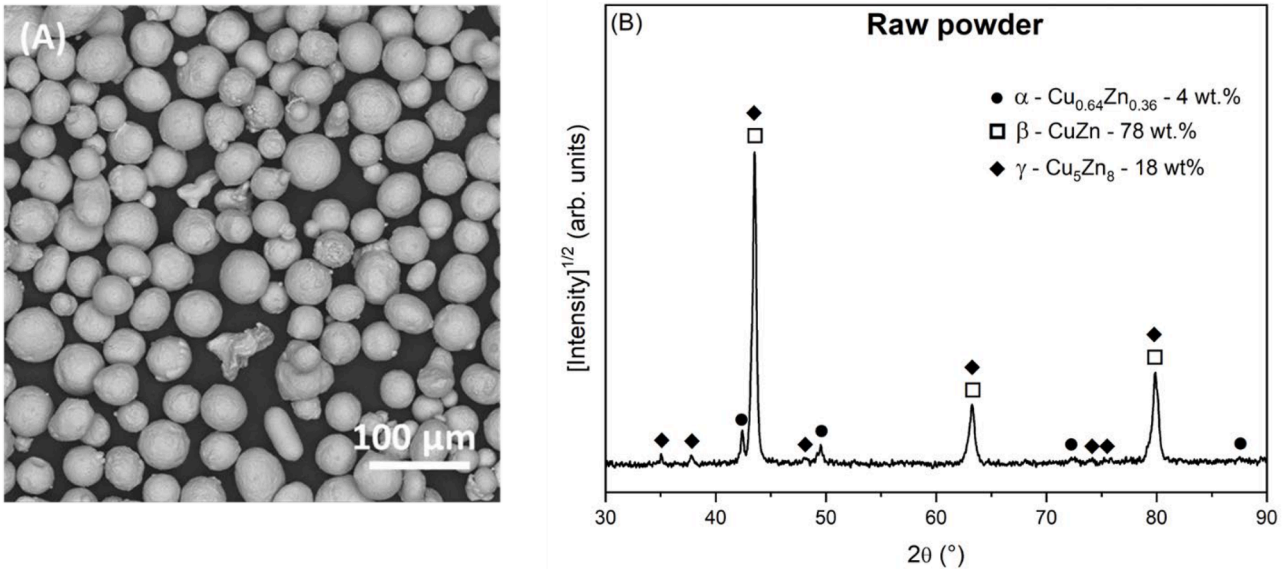

Fig. 2. Virgin raw powder: (A) SEM image and (B) XRD pattern with the weight fraction of phases provided by Rietveld refinement with MAUD software.

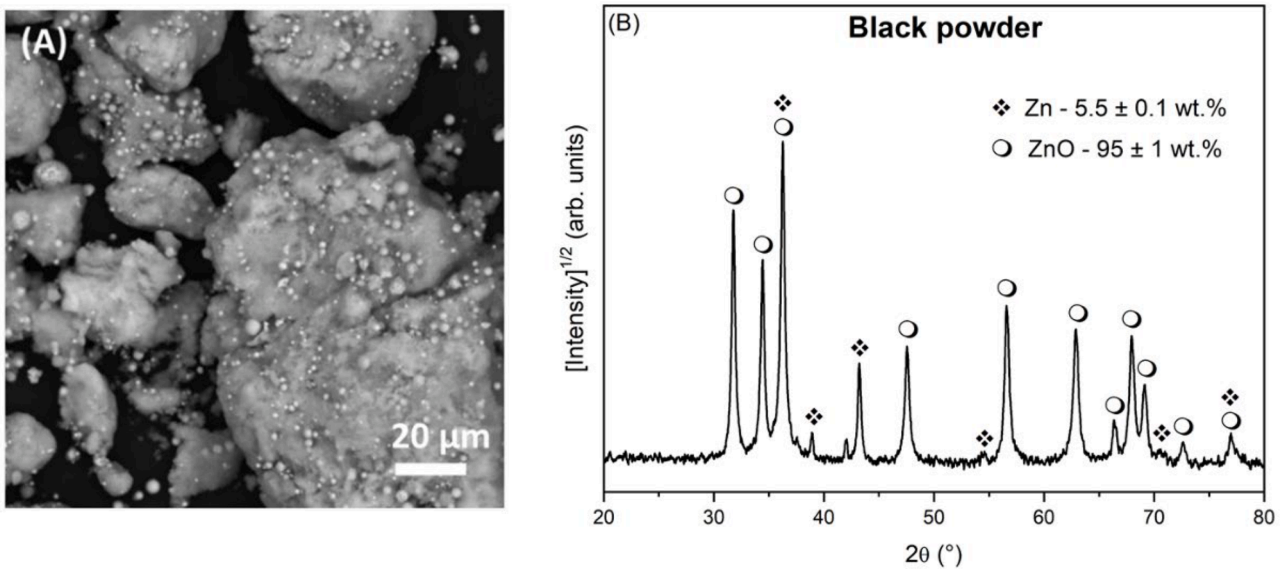

Fig. 3. Black powder collected in the filter: (A) SEM image and (B) XRD pattern with the weight fraction of phases and the experimental errors, provided by Rietveld refinement.

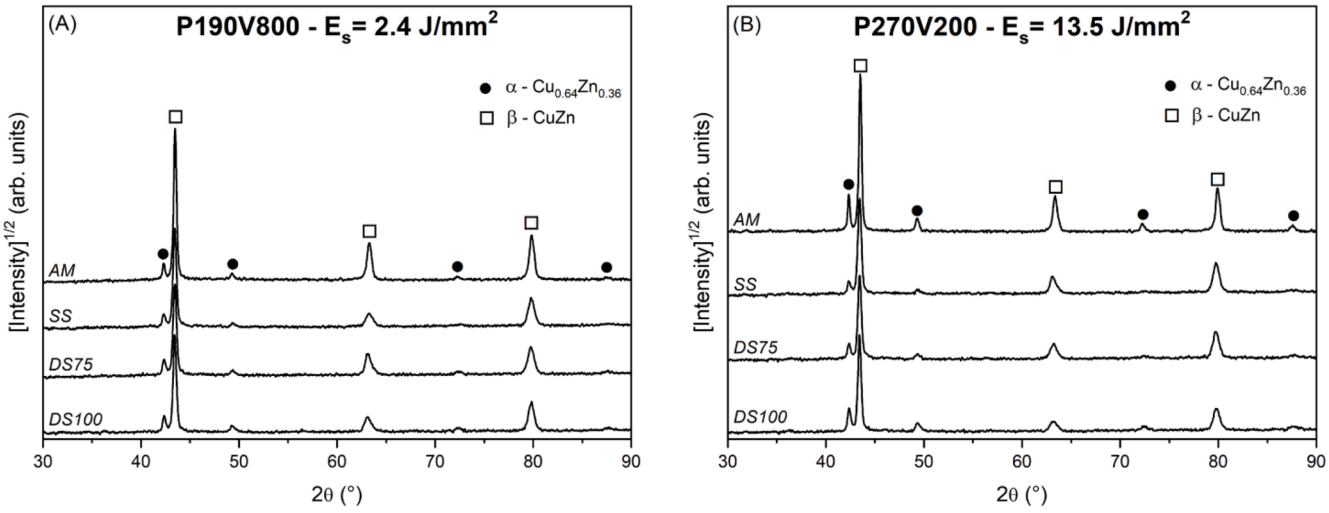

Fig. 4. XRD patterns of the as manufactured (AM) face and of the faces submitted to the different polishing treatments (SS, DS75, DS100): (A) sample manufactured at $P = 190$ W with the lowest value of SED ($E_s = 2.4$ J/mm^2) and (B) sample manufactured at $P = 270$ W with the highest value of SED ($E_s = 13.5$ J/mm^2). Patterns reported in square root intensity at the same full scale value.

Table 4
Variation of amount of α and β brass phases with the type of laser polishing treatment for samples deposited at the lowest and highest values of the surface energy density (SED) manufactured with laser power values of 190 W and 270 W, respectively. Results obtained by Rietveld refinement of the XRD patterns.

Brass phase	P190V800 – $E_s = 2.4$ J/mm^2				P270V200 – $E_s = 13.5$ J/mm^2			
	AM	SS	DS75	DS100	AM	SS	DS75	DS100
α-brass	1.6 ± 0.1	5.6 ± 0.2	8.2 ± 0.2	8.4 ± 0.2	12.5 ± 0.3	5.7 ± 0.2	9.0 ± 0.2	15.2 ± 0.2
β-brass	98 ± 3	94 ± 3	92 ± 2	92 ± 2	88 ± 2	94 ± 3	91 ± 2	85 ± 1

lower Zn content in the alloy due to Zn evaporation makes the formation of the α phase easier. This result shows that at the same value of the laser power (47 W) of the polishing treatment the microstructure of the sample is controlled by the laser frequency (Table 4).

SEM observations of the laser treated faces of samples P190V800 and P270V200 reported in Fig. 5 show that the polishing treatment refines the topography of the as manufactured surfaces with a progressive smoothing action from single step to double step laser ablation (Fig. 5).

SEM observations of the laser polishing effect on faces of samples P190V800 and P270V200 are reported in Fig. 5. Surface morphology depicted for as manufactured (AM) samples finds reason in the melting phase of the PBF-LB process, when the laser beam supplies sufficient energy to locally melt the powder. However, in areas close to the melted zone, the powder temperature remains below the melting point, resulting in numerous spherical CuZn42 particles being only partially bonded to the surface of the AM bulk samples. This creates the surface morphology depicted in Fig. 5A and 5B. Fig. 5C–5H show that the polishing treatment refines the topography of the as manufactured surfaces with a progressive smoothing action from single step to double step laser ablation. However, most original powder particles remain clearly distinguishable and new pores, previously concealed by partially melted particles, are unveiled.

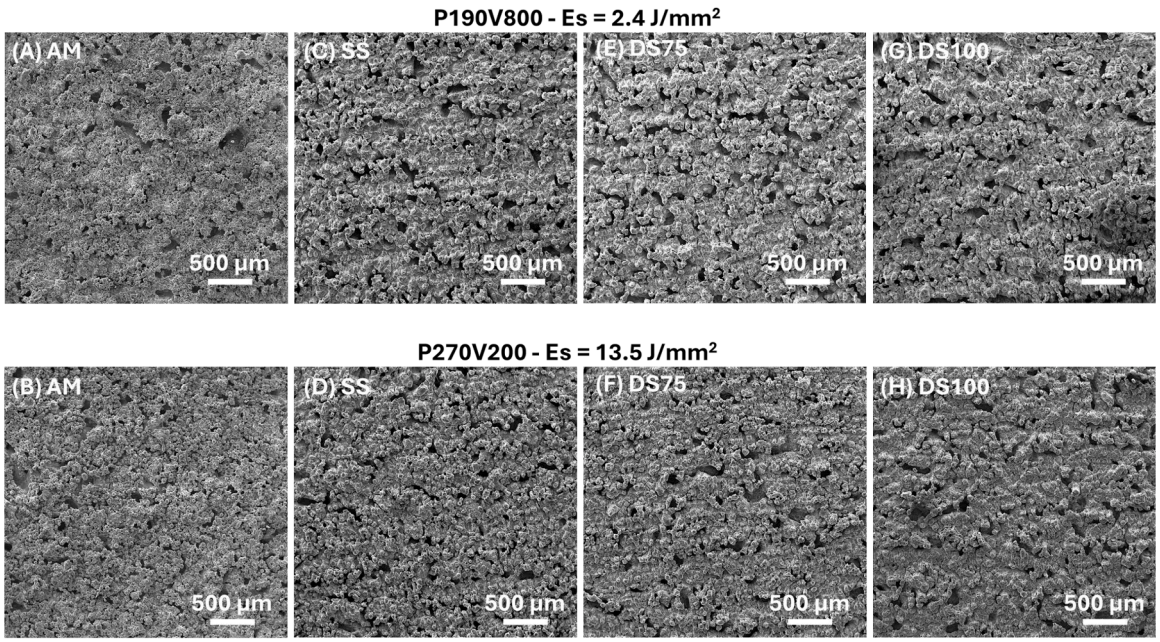

Fig. 5. SEM micrographs of lateral faces of samples P190V800 and P270V200 at low magnification (60x): AM (A and B); SS (C and D); DS75 (E and F) and DS100 (G and H).

The average surface roughness (Sa) of as manufactured samples (Fig. 6) exhibits a direct correlation with the process parameters. On increasing surface energy density (E_s), Sa decreases, up to E_s = 4.5 J/mm^2. DS100 laser treatment reduces the average surface roughness of AM samples. Particularly, from the difference curve in Fig. 6, calculated as AM-DS100, it is evident that the treatment is more effective when the sample is rougher, thus fabricated at lower surface energy density. For samples manufactured with higher values of surface energy density, ablation efficacy becomes independent of E_s.

The lack of standardized cleaning procedures for samples extracted from the build plate prior to roughness measurements presents challenges in comparing data across various studies. Nevertheless, some authors assert that the enhancement in surface quality achieved by laser polishing is localized, because of the limited size of the melt pool, which is insufficient to eliminate planarity deviations [27], as confirmed by SEM observations in Fig. 5. Ramos-Grez et al. [22] report the effectiveness of E_s = 30 J/mm^2 in reducing the roughness by at least 80 % over bronze-infiltrated stainless steel. Alfieri et al. [28] report the use of energy density ranging from 1 to 10 J/mm^2 resulting in a roughness reduction of 70 % at most on 316 L stainless steel. The roughness reduction measured in our study results lower than the reported literature data. In our study, the roughness reduction of the AM faces laser polished using DS100 treatment, is about 30 % for samples produced at lower surface energy density, up to 10 % for samples produced with higher E_s values (Fig. 6).

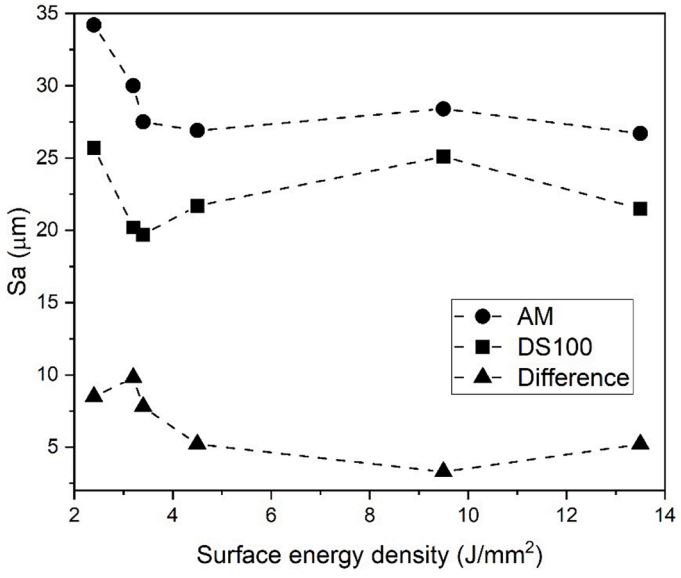

Fig. 6. Average surface roughness (Sa) of AM and DS100 VS surface energy density (E_s) used for manufacturing the specimens #1 to #6. Difference is calculated as AM-DS100.

Literature data evidenced two different laser polishing regimes: i) Surface shallow melting (SSM), where the thickness of the melted layer is lower than height of the surface asperities, from top to bottom. In this regime, the capillary pressure guides [29,30] material flow from peaks to local valleys; ii) Surface Over Melting (SOM), where the entire surface becomes liquid, and the surface tension gradient drives the formation of surface periodical structures. In laser polishing, surface shallow melting (SSM) prevails on surface over melting (SOM). Therefore, the surface peaks melt and fill the valleys generating a smoother surface, as visible from Fig. 5. In this work, the distribution of peaks and valleys of as manufactured and laser treated surfaces is described by the skewness (Ssk), while the kurtosis (Sku) measures the peak sharpness and valley depth. As shown in Fig. 7, surfaces show more valleys than peaks in as manufactured condition (Ssk $<$ 0). DS100 laser polishing results in flattening the peaks and softening the valleys, thus leading to a more symmetrical distribution of valleys and peaks (Ssk $\sim$ 0). Furthermore, AM faces present predominantly sharp peaks (Sku $>$ 3), that DS100 laser polishing smooths (Sku $\sim$ 3).

Sample produced with E_s = 13.5 J/mm^2 exhibits an anomalous behavior respect to the Ssk and Sku trend. This is likely due to E_s value above the process window within which fully dense samples were obtained in our previous work [9], identified in the range E_s= 2–10 J/mm^2 for the CuZn42 alloy. Above the process window, when the energy density is too high, a deposition condition known as “keyhole mode” is reached. In the keyhole regime, the melt pool is very deep and re-melting of multiple layers occurs. Within the process window, hardness values are strictly linked to density rather than to the type of brass phase [9]. Therefore, in our samples, the size of macroscopic defects

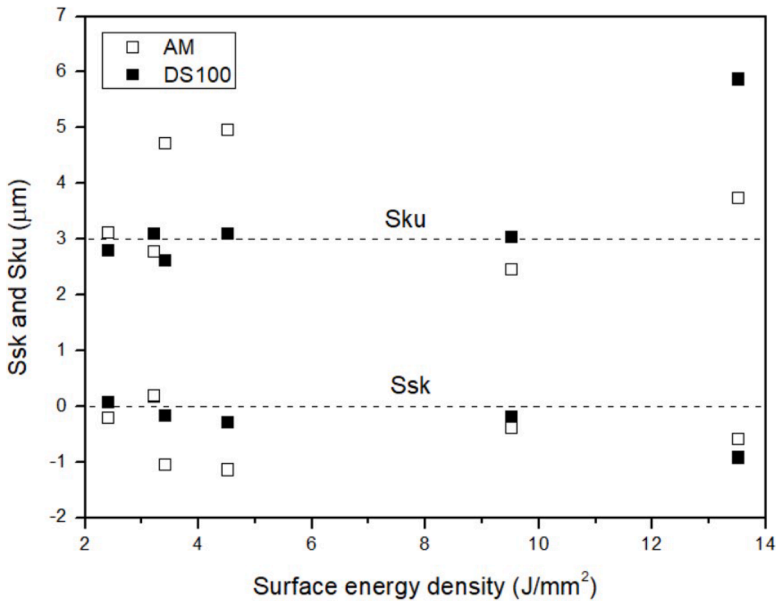

Fig. 7. Surface roughness parameters of skewness (Ssk) and kurtosis (Sku) of AM and DS100 VS surface energy density (E_s) used for manufacturing the specimens #1 to #6. Dashed lines indicate Ssk = 0 and Sku = 3.

determines both density and hardness values. Above $E_s = 10$ J/mm^2, both density and hardness drop because of larger internal cavities and pores [9]. Consequently, in the sample fabricated with $E_s = 13.5$ J/mm^2, porosity covered by semi-fused particles and satellites emerge after DS100 laser treatment. For this reason, valley distribution increases (Ssk < 0) and the sharpness of peak greatly rises (Ssk > 3).

Laser polishing also affects the chemical composition of sample surfaces (Fig. 8). EDS analysis of as manufactured surfaces in Fig. 8 reveals an increase in Zn concentration beyond the acceptance limit of 43 at.% [3], corresponding to a Zn/Cu ratio of 0.75. During PBF-LB process, spattered material, such as vapor or ejected particles, condenses or falls in the unmachined area or along the already solidified laser path. In this latter case, when the laser melts a layer, remelting typically 4–5 previous layers, facilitates the alloying of the condensed or fallen material in the melt pool, restoring a composition close to the original. Nevertheless, material sputtered at the borderline area may adhere to the component as larger particles or condense as zinc vapor, potentially contaminating the border and altering the chemical composition. Furthermore, the spattered material generated from the high vapor pressure elements, captured by the flow, results in a general loss of material, primarily zinc. This described mechanism induces a localized change in chemical composition. Therefore, the chemical composition of the surface may deviate from that of the bulk, which in turn may differ from the composition of the raw powder used. Therefore, AM surfaces require post processing finishing, in addition to aesthetic or tribological functions [31], for ensuring compliance with composition specifications. Laser polishing action melts the outer layer of the samples, leading to Zn evaporation. A lower Zn content in the laser treated alloy facilitates the

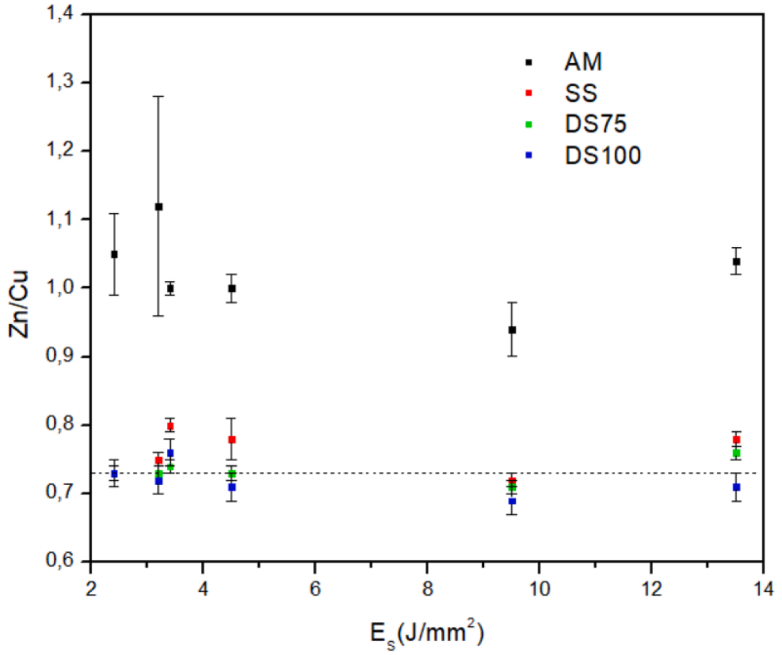

Fig. 8. Zn/Cu from EDS analysis VS surface energy density (E_s). The dashed line indicates the nominal Zn/Cu ratio (0.72).

formation of the α-phase, which is more deficient in zinc than the β-phase. Therefore, all samples exhibit an increase in weight loss of Zn based on the progressive laser frequency from 50 to 100 kHz (Fig. 8). The Zn/Cu ratio decrease results in an increase in the weight fraction of α-brass (Table 4). Moreover, laser polishing reduces the percentage of Zn to acceptable levels and aligns it with the nominal value of Zn/Cu ratio of the CuZn42 alloy (0.72).

Therefore, the target of laser polishing may be to restore chemical composition within prescribed limits, along with smoothing the initial topography, additionally offering the advantage of treating complex shapes without encountering issues related to environmental impact, prolonged processing times, high costs, and health risks for operators, as associated with alternative technologies [31].

4. Conclusions

This paper investigates the nature of the spattered powder and demonstrates that a laser polishing treatment can restore the standard chemical composition of the surface of a lead-free CuZn42 (CW510L) part produced by Laser Beam Powder Bed Fusion (PBF-LB). The results obtained can be summarized as follows:

- Exclusion of the cyclone pre-filter results in the formation of a "black powder" formed by large particles which exhibit a lower Zn/Cu ratio compared to small particles, thus indicating size-dependent variations of chemical composition influenced by spattering mechanisms;
- CuZn42 components produced by PBF-LB evidence an enrichment of the percentage of Zn on the external surface, causing the overcoming of the Zn/Cu limits for drinking water applications;
- Laser polishing treatments lead to a reduction in surface roughness, also confirmed by SEM investigation, with greater efficacy observed at lower surface energy densities;
- Laser polishing induces changes in surface chemical composition, primarily through Zn evaporation, leading to a decrease in Zn content and the restoration of chemical composition within prescribed limits;
- The increase in α-brass phase content post laser polishing is attributed to Zn evaporation induced by laser action, facilitating α-phase formation due to lower Zn content.

In conclusion, laser polishing presents a promising approach for enhancing the surface properties of CuZn42 alloy components, offering a balance between topographical refinement and chemical composition restoration.

CRediT authorship contribution statement

Andrea Gatto: Funding acquisition, Conceptualization. **Riccardo Groppo:** Methodology, Investigation. **Maria Laura Gatto:** Writing – original draft, Investigation. **Eleonora Santecchia:** Writing – review & editing, Supervision. **Daniel Munteanu:** Validation, Supervision. **Paolo Mengucci:** Writing – original draft, Formal analysis.

Declaration of competing interest

The authors declare that they have no known competing financial interests or personal relationships that could have appeared to influence the work reported in this paper.

Data availability

Data will be made available on request.

Acknowledgements

The authors would like to acknowledge the support received from the technicians of 3D4MEC SrL, Sasso Marconi, Bologna, Italy. This research was funded by 3D4MEC SrL, Sasso Marconi, Bologna, Italy and by Rubinetterie Bresciane Bonomi Spa, Via Massimo Bonomi, 1, 25064 Gussago BS.

References

[1] A. Vazdirvanidis, A. Rikos, A.I. Toulfatzis, G.A. Pantazopoulos, Electron backscatter diffraction (EBSD) analysis of machinable lead-free brass alloys: connecting texture with fracture, Metals 12 (4) (2022) 569.
[2] P. Stavroulakis, A.I. Toulfatzis, G.A. Pantazopoulos, A.S. Paipetis, Machinable leaded and eco-friendly brass alloys for high performance manufacturing processes: a critical review, Metals 12 (2) (2022) 246.
[3] Procedure for the acceptance of metallic materials for PDW - 14th Revision, 15th December 2020. ACCEPTANCE OF METALLIC MATERIALS USED FOR PRODUCTS IN CONTACT WITH DRINKING WATER, 4MS Common Approach.
[4] N. Zoghipour, E. Tascioglu, Y. Kaynak, Machinability of extruded and multi-directionally hot forged eco-friendly brass alloys, Can. Metall. Q. (2023) 1–12.
[5] J. Yin, W. Zhang, L. Ke, H. Wei, D. Wang, L. Yang, H. Zhu, P. Dong, G. Wang, X. Zeng, Vaporization of alloying elements and explosion behavior during laser powder bed fusion of Cu–10Zn alloy, Int. J. Mach. Tools Manuf. 161 (2021) 103686.
[6] H. Holden, Toxic materials in the electrical industry, Electron. Power 18 (11) (1972) 415–416.
[7] E.H. Greenhow, On brass-founders' ague, Med. Chir. Trans. 45 (1862) 177.
[8] A.I. Toulfatzis, G.A. Pantazopoulos, A.S. Paipetis, Fracture behavior and characterization of lead-free brass alloys for machining applications, J. Mater. Eng. Perform. 23 (2014) 3193–3206.
[9] A. Gatto, M.L. Gatto, R. Groppo, D. Munteanu, P. Mengucci, Influence of laser powder bed fusion process parameters on the properties of CuZn42 components: case study of the laser surface energy density, Prog. Addit. Manuf. 8 (5) (2023) 843–855.
[10] F. Hugger, K. Hofmann, S. Stein, M. Schmidt, Laser beam welding of brass, Phys. Procedia 56 (2014) 576–581.
[11] V.S. Kovivchak, T.V. Panova, K.A. Mikhailov, E.V. Knyazev, Modifying the composition of a brass and bronze surface layer under a high power ion beam of a nanosecond duration, Tech. Phys. Lett. 39 (2013) 59–62.
[12] A. Ur Rehman, M.A. Mahmood, P. Ansari, F. Pitir, M.U. Salamci, A.C. Popescu, I. N. Mihailescu, Spatter formation and splashing induced defects in laser-based powder bed fusion of AlSi10Mg alloy: a novel hydrodynamics modelling with empirical testing, Metals 11 (12) (2021) 2023.
[13] D. Wang, S. Wu, F. Fu, S. Mai, Y. Yang, Y. Liu, C. Song, Mechanisms and characteristics of spatter generation in SLM processing and its effect on the properties, Mater. Des. 117 (2017) 121–130.
[14] C. Liu, X. Mao, S.S. Mao, R. Greif, R.E. Russo, Particle size dependent chemistry from laser ablation of brass, Anal. Chem. 77 (20) (2005) 6687–6691.
[15] A.R. Nassar, M.A. Gundermann, E.W. Reutzel, P. Guerrier, M.H. Krane, M. J. Weldon, Formation processes for large ejecta and interactions with melt pool formation in powder bed fusion additive manufacturing, Sci. Rep. 9 (1) (2019) 5038.
[16] Z. Snow, A.R. Nassar, E.W. Reutzel, Invited Review Article: review of the formation and impact of flaws in powder bed fusion additive manufacturing, Addit. Manuf. 36 (2020) 101457.
[17] S.M. Basha, M. Bhuyan, M.M. Basha, N. Venkaiah, M.R. Sankar, Laser polishing of 3D printed metallic components: a review on surface integrity, Mater. Today Proc. 26 (2020) 2047–2054.
[18] A. Kumar, S. Saha, C.S. Kumar, A.K. Nath, Laser surface re-melting of additive manufactured samples with a line focused beam, Mater. Today Proc. 26 (2020) 1221–1225.
[19] J.P. Kruth, L. Froyen, J. Van Vaerenbergh, P. Mercelis, M. Rombouts, B. Lauwers, Selective laser melting of iron-based powder, J. Mater. Process. Technol. 149 (1–3) (2004) 616–622.
[20] K.C. Yung, W.J. Wang, T.Y. Xiao, H.S. Choy, X.Y. Mo, S.S. Zhang, Z.X. Cai, Laser polishing of additive manufactured CoCr components for controlling their wettability characteristics, Surf. Coat. Technol. 351 (2018) 89–98.
[21] S. Marimuthu, A. Triantaphyllou, M. Antar, D. Wimpenny, H. Morton, M. Beard, Laser polishing of selective laser melted components, Int. J. Mach. Tools Manuf. 95 (2015) 97–104.
[22] J.A. Ramos-Grez, D.L. Bourell, Reducing surface roughness of metallic freeform-fabricated parts using non-tactile finishing methods, Int. J. Mater. Prod. Technol. 21 (4) (2004) 297–316.
[23] K. Klages, C. Ruettimann, A. Olowinsky, Laser beam micro welding of dissimilar metals, in: Proceedings of the International Congress on Applications of Lasers & Electro-Optics, AIP Publishing, 2003.
[24] C. Meran, The joint properties of brass plates by friction stir welding, Mater. Des. 27 (9) (2006) 719–726.
[25] K. Klages, J. Gedicke, A. Olowinsky, Pulse forming at laser beam micro welding, in: Proceedings of the Pacific International Conference on Applications of Lasers and Optics, AIP Publishing, 2004.

[26] A. Gillner, A. Olowinsky, K. Klages, J. Gedicke, F. Sari, High-precision and high-speed laser microjoining for electronics and microsystems, in: Proceedings of the International Conference on Lasers, Applications, and Technologies 2005: Laser-Assisted Micro-and Nanotechnologies 6161, SPIE, 2006, pp. 10–20.
[27] Y. Tian, W.S. Gora, A.P. Cabo, L.L. Parimi, D.P. Hand, S. Tammas-Williams, P. B. Prangnell, Material interactions in laser polishing powder bed additive manufactured Ti6Al4V components, Addit. Manuf. 20 (2018) 11–22.
[28] V. Alfieri, P. Argenio, F. Caiazzo, V. Sergi, Reduction of surface roughness by means of laser processing over additive manufacturing metal parts, Materials 10 (1) (2016) 30.
[29] A. Lamikiz, J.A. Sánchez, L.L. de Lacalle, J.L. Arana, Laser polishing of parts built up by selective laser sintering, Int. J. Mach. Tools Manuf. 47 (12–13) (2007) 2040–2050.
[30] M. Vadali, C. Ma, N.A. Duffie, X. Li, F.E. Pfefferkorn, Pulsed laser micro polishing: surface prediction model, J. Manuf. Process. 14 (3) (2012) 307–315.
[31] B. Rosa, P. Mognol, J.Y. Hascoët, Laser polishing of additive laser manufacturing surfaces, J. Laser Appl. 27 (S2) (2015).